INCOHERENT ELECTRON CLOUD EFFECTS IN THE LARGE HADRON COLLIDER

K. Paraschou*,[1], G. Iadarola,
CERN, 1211 Geneva 23, Switzerland
[1]also at Aristotle University of Thessaloniki, 54124 Thessaloniki, Greece

Abstract

During the operation of the Large Hadron Collider in 2018, the majority of physics data was collected with a beam energy of 6.5 TeV, a bunch spacing of 25 ns and with β-functions in the high luminosity interaction points equal to 30 cm. In this configuration, it was found through several experimental measurements that electron cloud induces a significant degradation of the beam lifetime. This contribution reviews the available experimental observations, showing in particular the role played by the e-cloud located in regions around the interaction points, where the two beams share the same vacuum chamber. Recent developments toward a reliable numerical simulation of these incoherent effects driven by electron cloud are also presented.

INTRODUCTION

In the Large Hadron Collider (LHC), electron cloud (e-cloud) effects [1] manifest through different observables, especially when using the nominal bunch spacing of 25 ns. In particular, impacting electrons can induce increased heat loads on the beam screen of the superconducting magnets [2]; they can drive coherent instabilities [3]; they can absorb energy from the stored beam leading to longitudinal phase shifts [4]; and, due to their non-linear electromagnetic fields, they can increase particles' diffusion in the transverse phase space, causing slow emittance growth [5] as well as slow beam losses [6, 7].

This contribution is focused on the e-cloud effect on the slow continuous beam losses observed with colliding beams during the 2018 run (for a description of the LHC configuration and operation during that period see reference [8]).

In the first part we review the available experimental observations, collected during physics runs and special tests, which allow identifying e-cloud as a key source of the observed losses and to show the strong effect of the non-linearity introduced by e-cloud in the final-focusing quadrupoles (Inner Triplets - ITs). In the second part, we present ongoing development to achieve reliable simulations of these effects. A method is developed that uses a high-order local interpolation scheme to apply the e-cloud forces, computed by numerical simulations of the cloud dynamics, in a way that preserves the symplecticity of the beam particle motion.

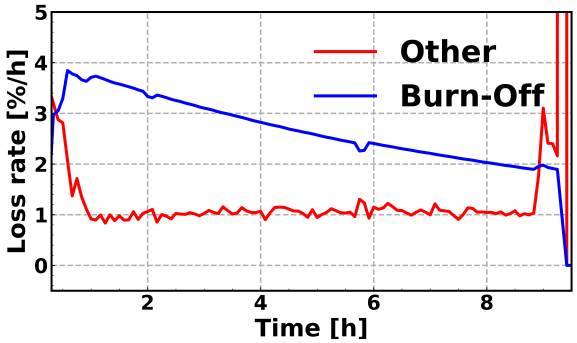

Figure 1: Beam losses from luminosity burn-off and from other sources during a typical LHC physics fill in 2018.

EXPERIMENTAL OBSERVATIONS

In this section we present the analysis of the LHC beam losses with colliding beams, based on bunch-by-bunch intensity measurements from the LHC Fast Beam Current Transformer. We will focus on the beam circulating in the clockwise sense (so-called beam 1). The other beam presents similar features in the beam losses, although often less pronounced.

When the beams are colliding, a significant fraction of protons are lost due to luminosity burn-off. To identify the proton loss rate driven by other sources, the burn-off loss rate is estimated from luminosity measurements and subtracted from the measured loss rate [9].

Observations for a typical physics fill

Figure 1 shows the burn-off loss rate (in blue) and the loss rate from other sources (in red) as they evolve during a typical physics fill, starting from the time at which the beams are brought in collision. It is possible to observe that, while burn-off losses gradually decrease during the fill following the luminosity decay, the additional losses exhibit a constant rate for most of the fill.

The LHC beam consists of several bunch trains separated by gaps of 800 ns between them. Each train is made of two or three batches of 48 bunches, with gaps of 200 ns between batches. Figure 2 shows the evolution of the loss rate for the different bunches in three consecutive trains. It is clear that bunches at the tails of the trains lose significantly more particles than those at the head of the trains, for the full duration of the fill. For all bunches the loss rate is practically constant during the fill. Stronger losses are observed at the beginning of the fill, right after collisions are established

* konstantinos.paraschou@cern.ch

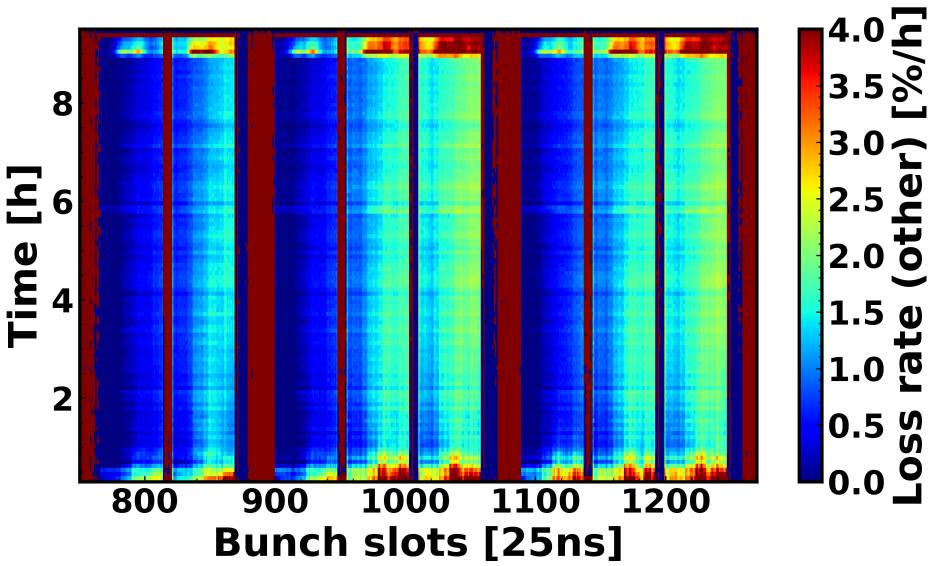

Figure 2: Bunch-by-bunch loss rate on three consecutive bunch trains during a typical LHC physics fill (loss rate from luminosity burn off is subtracted).

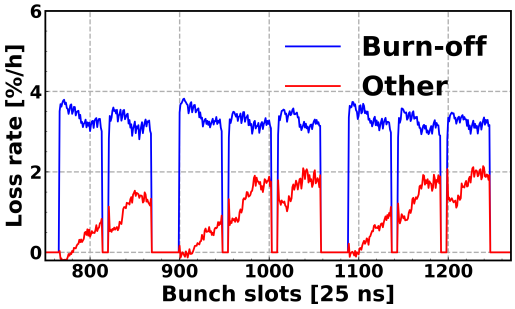

Figure 3: Comparison of the loss rates from burn-off and from other sources for the fill illustrated in Fig. 2 at the time $t = 2\,h$.

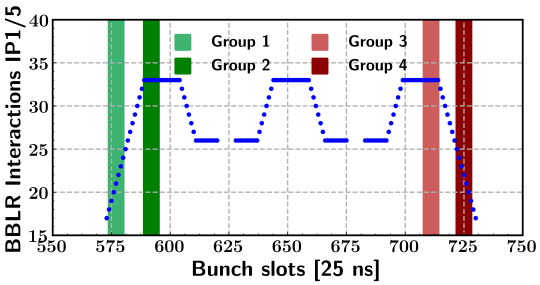

Figure 4: Number of BBLR interactions per interaction point for each bunch of a 3-batch train.

and towards the end of the fill, when the β-function at the two main experiments is reduced from 30 cm to 25 cm.

In Fig. 3, the bunch-by-bunch loss rates for burn-off and other sources are compared for a specific time ($t = 2\,h$). It is possible to notice that, while the burn-off rate is rather similar for all bunches, the additional losses strongly increase along the bunch train. Two main effects are expected to induce different loss rates for different bunches in the trains: e-cloud effects and Beam-Beam Long Range (BBLR) interactions [10].

To disentangle between these two effects, we select four groups of bunches along the trains (shown by the coloured bands in Fig. 4), having the following characteristics [6]:

Group 1: Bunches at the head of the leading batch of the train, experiencing the minimal amount of BBLR interactions and small e-cloud densities;

Group 2: Center of the leading batch of the train, experiencing the maximal amount of BBLR interactions and small e-cloud densities;

Group 3: Center of the trailing batch of the train, experiencing the maximal amount of BBLR interactions and large e-cloud densities;

Group 4: Tail of the trailing batch of the train, experiencing the minimal amount of BBLR interactions and large e-cloud densities.

Figure 5 shows the burn-off corrected losses as a function of time for these different groups of bunches. This analysis shows that the number of BBLR encounters has practically no impact on the observed losses, which instead tend to affect mostly the bunches at the tail of the trains. This observation points to e-cloud as the strongest source of the observed losses.

Effect of the crossing angle

During typical physics fills, in order to increase the integrated luminosity, the crossing angle between the two beams at the interaction points is gradually decreased from 320 μrad to 260 μrad, profiting from the fact that the BBLR interactions become weaker as the intensity of the beams decays [11].

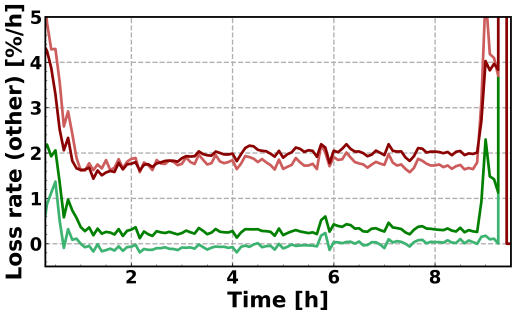

Figure 5: Loss rates measured for selected groups of bunches during a typical physics fill (color code defined in Fig. 4).

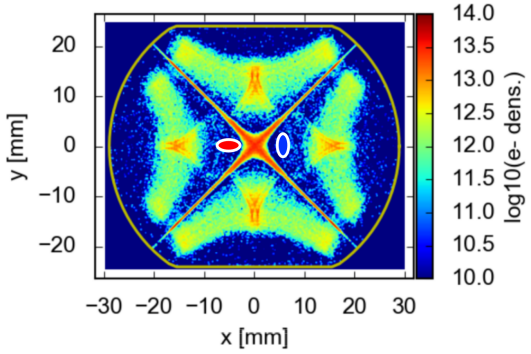

Figure 6: Electron density in one of the LHC IT quadrupoles (PyECLOUD simulation). The colored ellipses show the position and size of the two beams.

In addition to changing the strength of the BBLR interactions, a reduction in the crossing angle can also change the interaction of the beams with the e-cloud in regions close to the interaction points, by shifting the orbit of the beams to a region with different electron densities (see Fig. 6).

During a test fill, the crossing angle was kept constant at 320 μrad for the entire duration of the fill. The loss rates measured during this test are plotted in Fig. 7 with the same color code for the different bunch groups as in Fig. 5. Comparing Figs. 5 and 7, it is possible to observe a significant reduction of the loss rate when the crossing angle is kept constant, for all the bunch groups showing a visible loss rate. The fact that a dependence on the crossing angle is observed suggests that the e-cloud in the machine elements very close to the interaction point (in which a change in crossing angle results in a change in the electron density crossed by the beam) play a dominant role in generating the beam losses. The strongest e-cloud in the area develops in the LHC final-focusing quadrupoles (ITs) [12], and its effect on the beam is boosted by the extremely large β-function at their location.

Observations with a single circulating beam

In another dedicated experiment, the beam losses were recorded with a single circulating beam, with the same machine and beam configuration used for physics fills. Only a small train of 12 bunches was injected in the second ring for technical reasons.

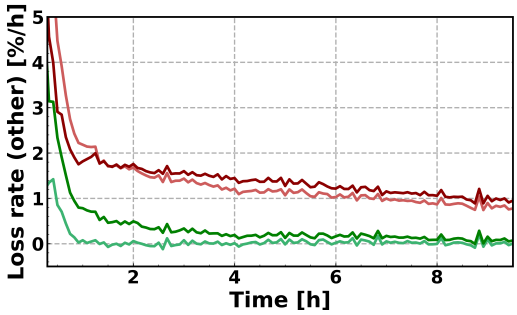

Figure 7: Loss rates measured for selected groups of bunches during a test fill performed with constant crossing angle (color code defined in Fig. 4).

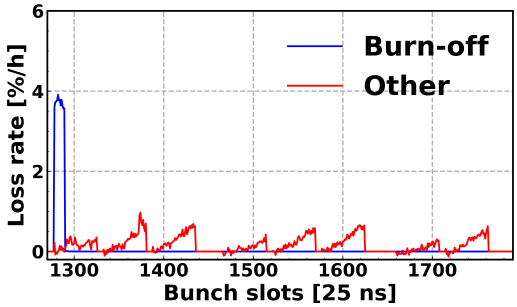

Figure 8: Loss rates measured with one circulating beam. In the other ring only 12 bunches are present, as it is visible on the burn-off trace.

The loss rates measured during this experiment are shown in Fig. 8. These can be compared against those measured during a typical physics fill as shown in Fig. 3. With a single beam, the losses are significantly smaller. This is mainly due to the suppression of the strong non-linear forces from the beam-beam head-on interactions at the four collision points and to a reduced e-cloud density in the presence of one beam alone. Still a clear pattern along the trains is observed on the measured loss rates. In particular it is possible to observe that, with a single beam, the loss rate decreases significantly after the 200-ns gap separating the three batches of a same train, while this is not the case with two circulating beams.

This is due to a characterizing feature of the e-cloud in the ITs, revealed by e-cloud build-up simulations shown in Fig. 9, which is due to the fact that in these elements the two beams circulate in the same vacuum chamber [12]. Figure 9 a shows that, with one circulating beam, the electron density decays significantly between consecutive batches. With two beams, instead, this does not happen since, during the passage of the gap of one beam, bunches of the other beam are present in the chamber. Comparing Fig. 9 a to Fig. 8 and Fig. 9 b to Fig. 3, one can recognize the similarity between the bunch-by-bunch pattern on the loss rate and the electron density simulations.

Tests with a different optics configuration

A confirmation of the fact that the losses are mainly driven by the e-cloud in the ITs is given by a test conducted to

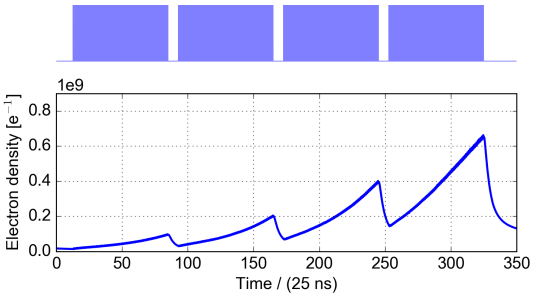

(a)

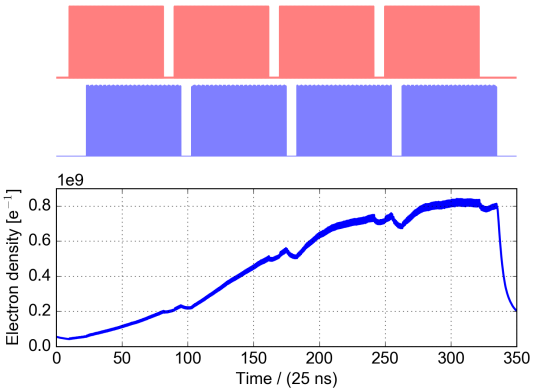

(b)

Figure 9: E-cloud build-up simulations with a) one beam and b) two beams in the common vacuum chamber of one of the IT quadrupoles.

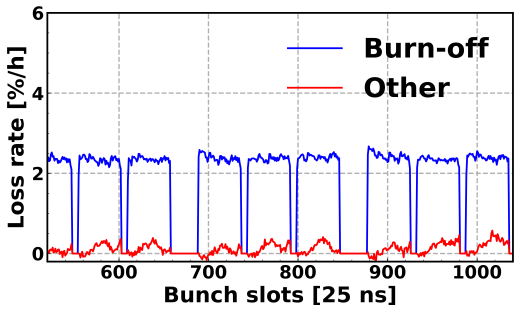

Figure 10: Bunch-by-bunch loss rates measured during a test fill with higher β-functions in the arcs and lower β-functions in the ITs.

validate a special beam optics configuration in preparation for the LHC Run 3 [13, 14].

During the test, the β-functions in half of LHC arcs were increased with respect to the configuration used for physics fills while the β-function in the ITs was significantly decreased (as the test was performed with larger β-function at the collision points). The measured bunch-by-bunch losses are shown in Fig. 10 and are much lower compared to those measured during typical physics fills as shown in Fig. 8. This can be ascribed to the fact that a reduced β-function at the ITs results in a weaker effect of the e-cloud at those locations.

SIMULATION OF INCOHERENT EFFECTS INDUCED BY ELECTRON CLOUD

The modelling and simulation of incoherent effects driven by e-cloud, has been addressed in the past by several authors. Benedetto et al. in [15] use maps recorded from a macroparticle simulation of the cloud dynamics to apply the e-cloud forces on the beam particles at each turn. As the maps are saved on a discrete grid, an interpolation scheme needs to be used to compute the forces at each turn. In general, as we will discuss in the following, the resulting kick can become artificially non-symplectic, which is known to generate artefacts on the simulated long-term dynamics of the beam particles [16]. Symplectic kicks can be obtained by using strongly simplified cloud distributions for which the kick can be expressed analytically, as done by Ohmi et al. in [17] or by Franchetti et al. in [18]. This approach on the other hand does not allow a realistic modelling of the cloud distribution, especially in the presence of dipolar and quadrupolar magnetic fields. To obtain a realistic model of the non-linear beam dynamics in the presence of e-cloud, which would allow simulating the very long time scales involved in the slow beam degradation illustrated in the previous section, we developed a numerical scheme that allows to apply a recorded field map in a way that preserves symplecticity. This approach will be presented in the following subsections, together with some numerical examples.

The electron cloud kick

It is possible to show [19] that, in the ultra-relativistic limit, the interaction of a beam particle with a short section of accelerator can be modelled with a "thin lens" map having the following form:

$$x \mapsto x \tag{1}$$

$$p_x \mapsto p_x - \frac{qL}{\beta_0 P_0 c}\frac{\partial \phi}{\partial x}(x, y, \tau) \tag{2}$$

$$y \mapsto y \tag{3}$$

$$p_y \mapsto p_y - \frac{qL}{\beta_0 P_0 c}\frac{\partial \phi}{\partial y}(x, y, \tau) \tag{4}$$

$$\tau \mapsto \tau \tag{5}$$

$$p_t \mapsto p_t - \frac{qL}{\beta_0 P_0 c}\frac{\partial \phi}{\partial \tau}(x, y, \tau) \tag{6}$$

where $\tau = \frac{s}{\beta_0} - ct$ and $p_t = \frac{E - E_0}{P_0 c}$ are canonically conjugate longitudinal variables, E is the energy of the particle, E_0, P_0 are the energy and momentum of the reference particle respectively, β_0 is the relativistic Lorentz factors of the reference particle, q is the charge of the interacting particle, L is the length of the interacting e-cloud, and $\phi(x, y, \tau)$ is the scalar potential describing the e-cloud, which can be obtained by solving a 2D Poisson problem.

For the simulation of collective instabilities driven by e-clouds the kick on the longitudinal momentum is typically

neglected and the kicks on the transverse momenta are computed by interpolating linearly a map defined on a discrete rectangular grid.

Although this algorithm is convenient to simulate instabilities, it is not suited to simulate slow beam losses. Its biggest drawback is the fact that the map is not symplectic for two reasons. The first reason is that since ϕ is dependent on all three variables x, y, τ, symplecticity is lost if the change in p_t is neglected. This however can easily be solved by simply applying also the longitudinal kick in Eq. 6.

The second reason is the fact that linear interpolation is used on a grid of derivatives of ϕ, estimated with finite differences. It is easy to show that the thin-lens map of Eq. 1-6 is symplectic if [20]:

$$\frac{\partial}{\partial x}\left(\frac{\partial \phi}{\partial y}\right) = \frac{\partial}{\partial y}\left(\frac{\partial \phi}{\partial x}\right) \tag{7}$$

$$\frac{\partial}{\partial y}\left(\frac{\partial \phi}{\partial \tau}\right) = \frac{\partial}{\partial \tau}\left(\frac{\partial \phi}{\partial y}\right) \tag{8}$$

$$\frac{\partial}{\partial \tau}\left(\frac{\partial \phi}{\partial x}\right) = \frac{\partial}{\partial x}\left(\frac{\partial \phi}{\partial \tau}\right) \tag{9}$$

These conditions would be satisfied automatically if the functions $\frac{\partial \phi}{\partial x}, \frac{\partial \phi}{\partial y}, \frac{\partial \phi}{\partial \tau}$ were analytical derivatives of a well behaved function $\phi(x, y, \tau)$, while they are in general not verified when using a linear interpolation scheme [20].

The conditions given by Eqs. 7 - 8, can be verified using a "tricubic interpolation" scheme [21]. In each grid cell, the potential ϕ is approximated by a third order polynomial:

$$\phi(x, y, \tau) = \sum_{i=0}^{3}\sum_{j=0}^{3}\sum_{k=0}^{3} a_{ijk} x^i y^j \tau^k \tag{10}$$

where the coefficients a_{ijk} change from cell to cell of the three-dimensional grid in a way that ensures continuity of the quantities:

$$\left\{\phi, \frac{\partial \phi}{\partial x}, \frac{\partial \phi}{\partial y}, \frac{\partial \phi}{\partial \tau}, \frac{\partial^2 \phi}{\partial x \partial y}, \frac{\partial^2 \phi}{\partial x \partial \tau}, \frac{\partial^2 \phi}{\partial y \partial \tau}, \frac{\partial^3 \phi}{\partial x \partial y \partial \tau}\right\} \tag{11}$$

To find the 64 coefficients a_{ijk}, the eight quantities of the set in Eq. 11 must be provided in all of the eight vertices of the cell. A finite difference scheme is employed to compute the required derivatives.

Application to a PyECLOUD simulation and mitigation of numerical artefacts

The method described above has been tested on a map generated by simulating the e-cloud dynamics using the PyECLOUD code [22, 23] (the initial distribution of electrons is uniform and there is no externally applied magnetic field). Figure 11 shows the horizontal field $E_x = -\frac{\partial \phi}{\partial x}$ close to the center of the chamber ($x = 0.027\sigma, y = 0$, with σ being the r.m.s. beam size) as a function of the longitudinal coordinate τ, as derived with finite differences on the grid (black points) and the result of the interpolation (red line).

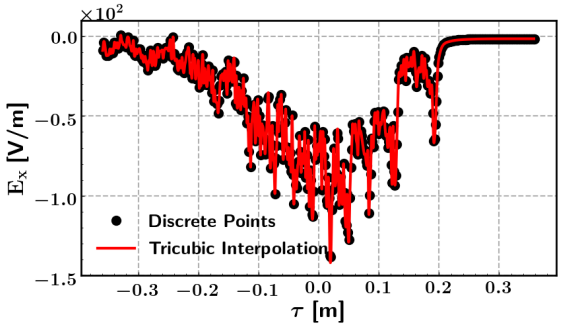

Figure 11: Horizontal field with respect to the longitudinal position for a beam particle close to the center of the beam chamber, as obtained from a single macroparticle simulation of the e-cloud dynamics.

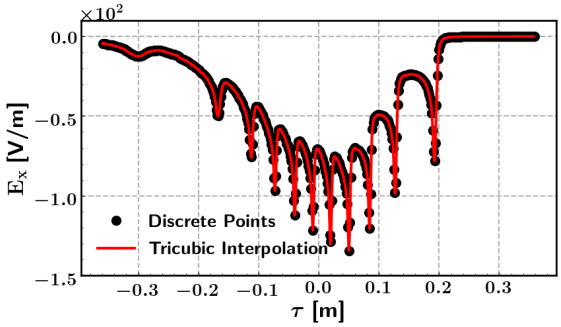

Figure 12: Horizontal field with respect to the longitudinal position for a beam particle close to the center of the beam chamber, as obtained from the average of 1000 macroparticle simulation of the e-cloud dynamics with different random seeds.

It is apparent that the simulation suffers from noise, as it can be expected from Particle-In-Cell macroparticle simulations. The noise can be effectively mitigated by averaging 1000 simulations with different random seeds. The result of the averaging shown in Fig. 12 uncovers the clear and physical structure of the modulated field produced by the e-cloud dynamics.

The interpolation technique shows some shortcomings in locations where the derivatives change rapidly. This can be seen in Fig. 13 where the horizontal field E_x is drawn against the horizontal position on the axial cut of the chamber ($y = 0$) during the passage of the synchronous particle ($\tau = 0$).

The source of these artefacts was identified to be the insufficient accuracy of the derivatives evaluated with the finite difference method. To acquire more accurate estimates of ϕ and its derivatives, we perform a linear interpolation of the electron charge distribution on a finer grid and we obtain a refined potential by solving Poisson's equation on such a grid. By applying the finite difference scheme on this new solution we also obtain better estimates of the derivatives.

To limit the memory consumption though, the new quantities $\left\{\phi, \frac{\partial \phi}{\partial x}, \frac{\partial \phi}{\partial y}, \frac{\partial \phi}{\partial \tau}, \frac{\partial^2 \phi}{\partial x \partial y}, \frac{\partial^2 \phi}{\partial x \partial \tau}, \frac{\partial^2 \phi}{\partial y \partial \tau}, \frac{\partial^3 \phi}{\partial x \partial y \partial \tau}\right\}$ are only kept on the original coarser grid. The result of this refine-

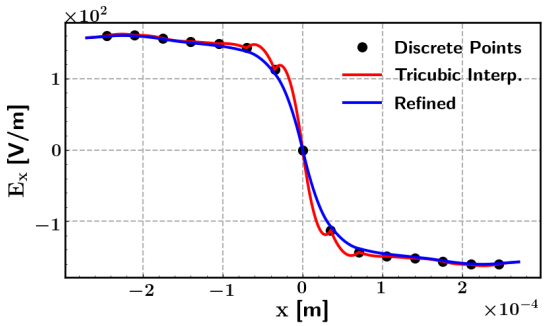

Figure 13: Horizontal field with respect to the horizontal position for a beam particle at $y = 0, \tau = 0$ before and after performing the refinement procedure.

ment algorithm is shown by the blue trace in Fig. 13, where it can be seen that the interpolation scheme no longer suffers from the "overshooting" artefacts [24].

To identify the effect of suppressing the artefacts, beam particles are tracked through a linear one-dimensional machine with Courant-Snyder parameters $\alpha_x = 2.3$, $\beta_x = 120\,m$, a tune of $Q_x = 0.3$ and a single e-cloud interaction. The structure of the horizontal phase space (Poincaré map) in normalized coordinates[1] is shown in Fig. 14 a when using the kick without the refinement and in Fig. 14 b when using the kick with the refinement. It is apparent that in Fig. 14 a the phase space shows considerably more (artificial) irregular motion between resonance islands compared to Fig. 14 b.

CONCLUSIONS

The measured loss rates observed at the LHC during 2018 collision fills exceeded by a significant fraction the expectations from luminosity burn-off.

The analysis of the loss rate at a bunch-by-bunch level shows that electron clouds are the main mechanism driving the observed beam losses. Dedicated experiments showing the sensitivity to the crossing angle, the behavior with a single circulating beam and the effect of the optics configuration, highlight the important role played by the e-cloud in the ITs.

To model and simulate these effects, a direct approach has been developed that uses symplectic maps based on a tricubic interpolation scheme, which is applied to e-cloud maps from macroparticle simulations. Special care had to be taken to suppress macroparticle noise and avoid interpolation artefacts. First tracking tests showed the importance of addressing these issues to have a reliable simulation of the beam particle motion.

[1] The normalized coordinates $(\hat{x}, \hat{p}_x)$ are related to the physical coordinates (x, p_x) through $\begin{pmatrix} \hat{x} \\ \hat{p}_x \end{pmatrix} = \begin{pmatrix} \frac{1}{\sqrt{\beta_x}} & 0 \\ \frac{\alpha_x}{\sqrt{\beta_x}} & \sqrt{\beta_x} \end{pmatrix} \begin{pmatrix} x \\ p_x \end{pmatrix}$

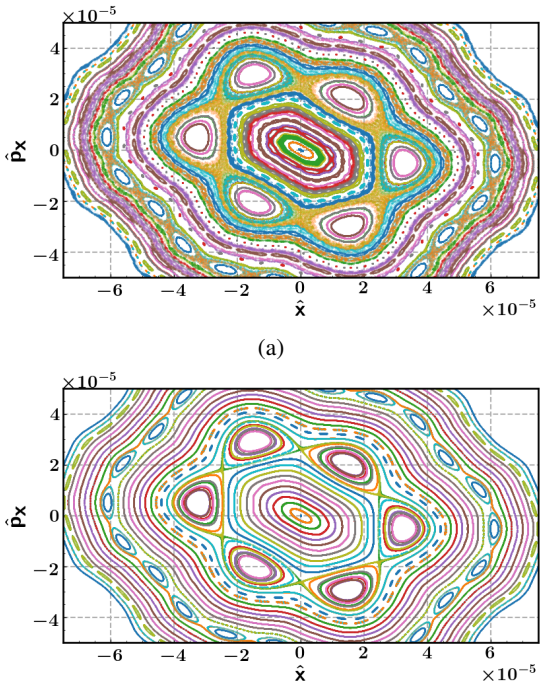

(a)

(b)

Figure 14: Normalized phase space $(\hat{x} - \hat{p_x})$ of particles tracked with the e-cloud map without (a) and with (b) the refinement procedure. Different colors correspond to particles tracked with different initial conditions.

ACKNOWLEDGEMENTS

The authors would like to thank F. Antoniou, G. Arduini, H. Bartosik, I. Efthymiopoulos, S. Fartoukh, N. Karastathis, S. Kostoglou, E. Métral, Y. Papaphilippou, D. Pellegrini, G. Rumolo, G. Sterbini for their important input and support to the presented work.

REFERENCES

[1] G. Iadarola and G. Rumolo, "Electron cloud effects", in *Proc. ICFA Mini-Workshop on Impedances and Beam Instabilities in Particle Accelerators*, Benevento, Italy, Sep. 2018, pp. 49–56. doi:10.23732/CYRCP-2018-001.49

[2] G. Skripka *et al.*, "Comparison of Electron Cloud Build-Up Simulations Against Heat Load Measurements for the LHC Arcs With Different Beam Configurations", in *Proc. 10th Int. Particle Accelerator Conf. (IPAC'19)*, Melbourne, Australia, Jun. 2019, pp. 3232–3235. doi:10.18429/JACoW-IPAC2019-WEPTS051

[3] A. Romano *et al.*, "Electron cloud buildup driving spontaneous vertical instabilities of stored beams in the Large Hadron Collider", *Phys. Rev. ST Accel. Beams*, vol. 21, pp. 061002, Jun. 2018. doi:10.1103/PhysRevAccelBeams.21.061002

[4] Esteban Müller, J. F. *et al.*, "High-accuracy diagnostic tool for electron cloud observation in the LHC based on synchronous phase measurements", *Phys. Rev. ST Accel. Beams*, vol. 18, pp. 112801, Nov. 2015. doi:10.1103/PhysRevSTAB.18.112801

[5] S. Papadopoulou *et al.*, "Monitoring and Modelling of the LHC Emittance and Luminosity Evolution in 2018", in *Proc. 10th Int. Particle Accelerator Conf. (IPAC'19)*, Melbourne, Australia, Jun. 2019, pp. 3212–3215. doi:10.18429/JACoW-IPAC2019-WEPTS046

[6] K. Paraschou *et al.*, "Analysis on Bunch-by-Bunch Beam Losses at 6.5 TeV in the Large Hadron Collider", in *Proc. 10th Int. Particle Accelerator Conf. (IPAC'19)*, Melbourne, Australia, Jun. 2019, pp. 500–503. doi:10.18429/JACoW-IPAC2019-MOPMP029

[7] S. Kostoglou *et al.*, "Luminosity, lifetime and modelling ", presented at the 9th LHC Operations Evian Workshop, Evian, France, Jan. 2019. https://indico.cern.ch/event/751857/contributions/3259405/.

[8] J. Wenninger, "Operation and configuration of the LHC in run 2", CERN, Geneva, Switzerland, Rep. CERN-ACC-NOTE-2019-0007, Mar. 2019.

[9] N. Karastathis *et al.*, "Monitoring and modeling of the LHC luminosity evolution in 2017", in *Proc. 9th Int. Particle Accelerator Conf. (IPAC'18)*, Vancouver, BC, Canada, Apr.–May 2018, pp. 224–227. doi:10.18429/JACoW-IPAC2018-MOPMF052

[10] W. Herr *et al.*, "Long range beam-beam effects in the LHC", in *Proc. ICFA Mini-Workshop on Beam-Beam Effects in Hadron Colliders (BB2013)*, CERN, Geneva, Switzerland, Mar. 2013, pp. 87–92. doi:10.5170/CERN-2014-004.87

[11] N. Karastathis *et al.*, "Crossing Angle Anti-Leveling at the LHC in 2017", in *Proc. 9th Int. Particle Accelerator Conf. (IPAC'18)*, Vancouver, BC, Canada, Apr.–May 2018, pp. 184–187. doi:10.18429/JACoW-IPAC2018-MOPMF040

[12] G. Skripka, G. Iadarola and A. Romano, "Electron cloud build up in two-beam regions for HL-LHC: heat load and vacuum aspects", presented at ECLOUD'18, Elba, Italy, Jun. 2018. Proceeding to be published. https://agenda.infn.it/event/13351/contributions/18959/.

[13] S. Fartoukh, "Achromatic telescopic squeezing scheme and application to the LHC and its luminosity upgrade", *Phys. Rev. ST Accel. Beams*, vol. 16, pp. 111002, Nov. 2013. doi:10.1103/PhysRevSTAB.16.111002

[14] S. Fartoukh, A. Mereghetti and M. Solfaroli, "MD3270 Round ATS + MD4023 TCDQ levelling", presented at the LHC Studies Working Group meeting, CERN, Geneva, Switzerland, Nov. 2018. https://indico.cern.ch/event/772189/contributions/3209049/.

[15] E. Benedetto *et al.*, "Incoherent Effects of Electron Clouds in Proton Storage Rings", *Phys. Rev. Lett.*, vol. 97, pp. 034801, Jul. 2006. doi:10.1103/PhysRevLett.97.034801

[16] W. Herr, "Mathematical and Numerical Methods for Nonlinear Beam Dynamics", in *CAS - CERN Accelerator School: Advanced Accelerator Physics Course*, Trondheim, Norway, Aug. 2013, pp.157–198. doi:10.5170/CERN-2014-009.157

[17] K. Ohmi and K. Oide, "Chaos and emittance growth due to nonlinear interactions in a circular accelerator", *Phys. Rev. ST Accel. Beams*, vol. 10, pp. 014401, Jan. 2007. doi:10.1103/PhysRevSTAB.10.014401

[18] G. Franchetti *et al.*, "Incoherent effect of space charge and electron cloud", *Phys. Rev. ST Accel. Beams*, vol. 12, pp. 124401, Dec. 2009. doi:10.1103/PhysRevSTAB.12.124401

[19] G. Iadarola, "Modelling the interaction of a relativistic beam particle with an electron cloud ", CERN, Geneva, Switzerland, Rep. CERN-ACC-NOTE-2019-0033, Aug. 2019. https://cds.cern.ch/record/2684858/.

[20] K. Paraschou, G. Iadarola, "Symplectic kicks from an e-cloud pinch", presented at Electron Cloud Meeting #67, CERN, Geneva, Switzerland, Nov. 2019. https://indico.cern.ch/event/811014/contributions/3379525/.

[21] F. Lekien and J. E. Marsden, "Tricubic Interpolation in Three Dimensions", *Int. J. Numer. Meth. Engng.*, vol. 63, pp.455—471, Mar. 2005. doi:10.1002/nme.1296

[22] G. Iadarola *et al.*, "Evolution of Python Tools for the Simulation of Electron Cloud Effects", in *Proc. 8th Int. Particle Accelerator Conf. (IPAC'17)*, Copenhagen, Denmark, May 2017, pp.3803–3806. doi:10.18429/JACoW-IPAC2017-THPAB043

[23] G. Iadarola *et al.*, "PyECLOUD". https://github.com/PyCOMPLETE/PyECLOUD/.

[24] K. Paraschou, G. Iadarola, "Update on development for single-particle tracking with e-cloud", presented at Electron Cloud Meeting #72, CERN, Geneva, Switzerland, Nov. 2019. https://indico.cern.ch/event/862798/contributions/3635364/.